

# Computational pharmacokinetics/pharmacodynamics of rifampin in a mouse tuberculosis infection model

Michael A. Lyons<sup>1</sup> · Anne J. Lenaerts<sup>1</sup>

Received: 20 January 2015 / Accepted: 25 May 2015 / Published online: 31 May 2015  
© Springer Science+Business Media New York 2015

**Abstract** One critical approach to preclinical evaluation of anti-tuberculosis (anti-TB) drugs is the study of correlations between drug exposure and efficacy in animal TB infection models. While such pharmacokinetic/pharmacodynamic (PK/PD) studies are useful for the identification of optimal clinical dosing regimens, they are resource intensive and are not routinely performed. A mathematical model capable of simulating the PK/PD properties of drug therapy for experimental TB offers a way to mitigate some of the practical obstacles to determining the PK/PD index that best correlates with efficacy. Here, we present a preliminary physiologically based PK/PD model of rifampin therapy in a mouse TB infection model. The computational framework integrates whole-body rifampin PKs, cell population dynamics for the host immune response to *Mycobacterium tuberculosis* infection, drug-bacteria interactions, and a Bayesian method for parameter estimation. As an initial application, we calibrated the model to a set of available rifampin PK/PD data and simulated a separate dose fractionation experiment for bacterial killing kinetics in the lungs of TB-infected mice. The simulation results qualitatively agreed with the experimentally observed PK/PD correlations, including the identification of area under the concentration-time curve as best correlating with efficacy. This single-drug framework is aimed toward extension to multiple anti-TB drugs in order to facilitate development of optimal combination regimens.

**Keywords** Rifampin · PKPD · Tuberculosis · Mice · Immune response · Modeling

## Introduction

A major aim of anti-tuberculosis (anti-TB) drug development is the identification of new combination regimens to better treat drug-susceptible and drug-resistant TB, including TB in human immunodeficiency virus (HIV) co-infected patients [1]. In order to accelerate the development process relative to sequential single-drug replacement in current three- and four-drug regimens, a critical path to TB drug regimens (CPTR) initiative is underway in which the unit of development is an entirely novel multidrug combination [2]. Presently, several novel anti-TB drug combinations have been tested in mice [3–5] and a first multidrug early bactericidal activity (EBA) study has been completed in humans [6].

Beyond the identification of specific drugs to test in combination, there remains the problem of dose optimization which is important both for the therapeutic benefits and as a means to conserve the effective use of the drugs [7]. However, the problem of identifying optimized regimens for TB is especially difficult due in part to the large number of possible doses and schedules of administration that arise from multidrug combinations, but also due to an incomplete understanding of the relationships among the set of pharmacokinetic (PK), pharmacodynamic (PD), and disease related elements that influence the outcomes of the relevant experiments. These difficulties are illustrated by the continuing investigations of standard anti-TB regimens that have been in clinical use for more than 30 years [8–10]. Our focus here is dose optimization in mouse TB infection models, as they are the primary animal models in the noted regimen-based initiative [11].

✉ Michael A. Lyons  
michael.lyons@colostate.edu

<sup>1</sup> Department of Microbiology, Immunology and Pathology,  
Colorado State University, Fort Collins, CO, USA

Antimicrobial PK/PD methods provide the current basis for preclinical dose optimization of single anti-TB drugs [12–14]. These methods include measurements and analysis of drug concentration–time profiles and dose fractionation studies to determine correlations between efficacy and various PK/PD indices descriptive of drug exposure and effect. Although preclinical PK/PD data have been informative for optimal dosing in TB patients [15], the resource intensive requirements of in vivo anti-TB PK/PD studies often leads to their consideration as a secondary investigation; for example, following an unexpected pattern of drug behavior observed in clinical testing [16]. The multidimensional exposure–efficacy relationships needed to characterize the three- and four-drug combinations used to treat TB would require even greater experimental resources. Preclinical anti-TB combination studies are currently performed using a limited range of doses that are determined primarily from single-drug studies for new drugs, or from previously optimized regimens for existing drugs [4, 17].

Mathematical modeling and simulation provides a complementary approach to experimental methods that may mitigate some of the practical obstacles to combination regimen based development. Compartmental PK/PD modeling is the most commonly used approach to describe and predict drug exposure–efficacy relationships [18]. These models, typically consisting of one or more compartments for drug concentration kinetics combined with effect compartments for the drug–bacteria interaction, have been used to predict optimal PK/PD indices for a variety of antimicrobial drugs in both in vitro and in vivo systems [19–21]. However, these conventional PK/PD models aim at reducing the complexity of the drug–biological system interactions to a minimal set of free parameters whose values are specified by data from the types of experiments that are to be simulated. This limits their application to quantitative descriptions of a relatively small number of model variables with a narrowly defined set of experimentally measurable endpoints. In contrast, physiologically based PK/PD models [22] incorporate mechanistic descriptions of the exposure–efficacy relationships using variables and parameters that have physiological and biochemical interpretations. This provides for the experimental measurement of internal model components and a predictive capability beyond the experimental designs used for model development.

As a step toward a mathematical and computational modeling framework capable of describing and predicting PK/PD relationships for preclinical anti-TB regimen-based development, we constructed a physiologically based PK/PD model for rifampin in *Mycobacterium tuberculosis* infected mice, including a population model for the host-immune response to infection. As an initial application, we calibrated the model to a subset of experimental data from

a rifampin PK/PD study in mice by Jayaram et al. [12] and simulated a separate dose fractionation experiment to determine an optimal PK/PD index for efficacy of rifampin against TB-infected mice.

## Materials and methods

### Pharmacokinetic/pharmacodynamic model

The mathematical PK/PD model was constructed by combining a physiologically based pharmacokinetic (PBPK) model for rifampin in mice [23] with a host-effect model (TB model) describing *M. tuberculosis* infection in the lungs of mice [24]. The PBPK model provided rifampin concentration–time profiles for the major tissues and organs, including plasma and lungs, for single and multiple oral dosing. The TB model provided the dynamics in the lungs of (1) intra- and extra-cellular bacteria, (2) resting, activated, and infected macrophages, (3) CD4<sup>+</sup> and CD8<sup>+</sup> T cells, and (4) the cytokines IL-2, IL-10, IL-12, and IFN- $\gamma$ . Both the PBPK and TB models consisted of physiologically parameterized ordinary differential equations, and the two models were combined through terms for drug-induced killing of the intra- and extra-cellular bacteria.

The drug–bacteria interaction in the lungs was described with a sigmoidal killing term [25] added to the existing equations for bacterial dynamics given in Friedman et al. [24]; these new equations for bacterial cell density ( $B$ ) as a function of time ( $t$ ) took the form,

$$\frac{dB}{dt} = \frac{dB}{dt} \Big|_{Host} - B \cdot k_{max} \cdot \frac{(f_{LU} \cdot C_{LU})^\gamma}{EC_{50}^\gamma + (f_{LU} \cdot C_{LU})^\gamma} \quad (1)$$

The total rifampin concentration in lungs,  $C_{LU}$  (with  $f_{LU}$  the corresponding free fraction), was determined from the PBPK model equation,

$$V_{LU} \frac{dC_{LU}}{dt} = Q_C (C_V - C_{LU}/P_{LU}), \quad (2)$$

where  $V_{LU}$  is lung tissue volume,  $Q_C$  is cardiac output,  $C_V$  is rifampin concentration in venous blood, and  $P_{LU}$  is the rifampin lung/blood partition coefficient. There were three bacterial cell density equations described by (1); one each for extracellular bacteria and intracellular bacteria in activated or infected macrophages. The first term on the right-hand side of Eq. (1) represents the bacterial dynamics in the host environment in the absence of drug, with the explicit form for each of the three bacterial subpopulations given by the corresponding equations in Friedman et al. [24]. The drug effect parameters,  $k_{max}$ ,  $EC_{50}$ , and  $\gamma$ , represent the maximum kill rate, half-maximum effect drug concentration, and Hill coefficient, respectively. These parameters were further distinguished as corresponding to

either extracellular bacteria,  $Ex$ , or intracellular bacteria,  $In$  (for bacteria inside either activated or infected macrophages); in the equation for extracellular bacteria,  $k_{max} = k_{max}^{Ex}$ ,  $EC_{50} = EC_{50}^{Ex}$ , and  $\gamma = \gamma^{Ex}$ , and for both equations describing intracellular bacteria,  $k_{max} = k_{max}^{In}$ ,  $EC_{50} = EC_{50}^{In}$ , and  $\gamma = \gamma^{In}$ .

The complete set of PK/PD model equations were obtained by combining all the equations listed in the respective publications for the separate PBPK [23] and TB [24] models into a single model structure, with the only modification being to the three original bacterial dynamics equations to include drug-induced bacterial killing as described above. A diagram of the complete model structure together with the full set of equations is given in the “Appendix” section. We refer the reader to the original model publications [23, 24] for additional equation details. The complete set of parameter values were specified first as baseline values, followed by modification of some of these values through model calibration to various sets of in vivo experimental data. The initial conditions for the TB model were specified in Friedman et al. [24] at day seven of infection, with values appropriate for low-dose aerosol exposure to *M. tuberculosis*. The initial drug concentrations in all PBPK model compartments were set to zero.

### Baseline parameter values

Baseline values for the TB model parameters and the initial cell densities and cytokine concentrations, were chosen as those specified for young mice in Friedman et al. [24]. With the exception of mean body weight, baseline values for the PBPK model parameters were chosen as the mean values listed in Lyons et al. [23]. Mean body weight was set to 21 g [26] as representative of the 7- to 9-week old male and female BALB/c mice used for the in vivo measurements in Jayaram et al. [12]. A baseline value for  $f_{LU}$  was set from the rifampin unbound fraction in plasma ( $f_{plasma}$ ) obtained from Jayaram et al. [12], as  $f_{LU} = f_{plasma} \cdot BP/P_{LU}$  [27], where  $BP$  is the rifampin blood/plasma ratio, and  $P_{LU}$  is the rifampin lung/blood partition coefficient. Baseline values for the drug effect parameters were set from the corresponding terms in the dose–response curves for in vitro killing kinetics assays given in Jayaram et al. [12]; the batch culture results were used for the extracellular values, and the macrophage infection model results were used for the intracellular values.

### Model calibration

The PK/PD model calibration was performed using a Bayesian Markov chain Monte Carlo (MCMC) procedure [28, 29] applied sequentially to a set of in vivo data for

rifampin in BALB/c mice reported in Jayaram et al. [12]. A first calibration to dose-ranging pharmacokinetic data in uninfected mice was followed by a second calibration to dose–response data in *M. tuberculosis* aerosol infected mice.

The data obtained from the in vivo dose-ranging and dose–response studies in Jayaram et al. [12] consisted of, respectively; (1) mean values for 72-h rifampin plasma concentration-time measurements after single oral doses of 0.33, 10, 90, 270, and 810 mg/kg, and (2) mean lung CFU counts from mice treated with rifampin for 1 or 2 weeks, where treatment started on day 28 of infection using doses in a range of 1–270 mg/kg, administered orally 6 days/week. The numerical values for these data were obtained here from the corresponding published graphs by digital extraction using *g3data* [30, 31] [we note that the original individual data were not available (R. Shandil, personal communication)]. The 72-h rifampin plasma concentration-time measurements corresponding to the 10, 90, and 270 mg/kg doses were chosen as the calibration data from the dose-ranging study, consistent with the results in Jayaram et al. [12] indicating that a non-compartmental model with a 12-h elimination half-life best described the mouse pharmacokinetics. The dose–response data exhibited a large amount of variability over the 2-week treatment interval, particularly in the low doses; as such, we limited the calibration data to the 1-week treatment group with lung CFU counts measured on days 28 and 35 post infection.

The model parameters chosen for calibration were those in the drug–bacteria interaction terms, for which the baseline values were specified using in vitro data, together with additional parameters that were found to most sensitively affect model predictions for rifampin plasma concentration and total bacterial cell density (the latter was calculated as the sum of the intra- and extra-cellular subpopulations). The sensitive parameters were identified using a Monte Carlo (MC) sensitivity analysis, where each MC iteration consisted of a simulation of the time-course of chosen model variables, with the parameter values set by random draws from uniform distributions bounded by  $\pm 10\%$  of their baseline mean values. Parameter sensitivity was assessed from correlation coefficients calculated, at specified time points, between the sampled parameter values and model output resulting from 10,000 MC iterations.

The Bayesian procedure included the specification of prior parameter distributions, a likelihood function, and an error term accounting for model and measurement uncertainty. For those parameters subject to calibration, the prior distributions were chosen as uniform,  $U(M - \sqrt{3} \cdot SD, M + \sqrt{3} \cdot SD)$ , with mean ( $M$ ) set to the baseline parameter value, and standard deviation ( $SD$ ) set from a coefficient of variation ( $CV = SD/M$ ) chosen from a range of 30–50 % to represent the

uncertainty in the mean (the  $\sqrt{3}$  arises from parameterization of  $U$  in terms of  $M$  and  $SD$ ). All other model parameters that were not subject to calibration were held at their baseline values (see “Appendix” section). The calibration was implemented using MCMC simulation, with log-transformed experimental calibration data, and a normal likelihood with a loguniform error variance bounded between 0.01 and 3.3 [32]. The joint posterior parameter distribution was sampled using five independent Markov chains, with convergence assessed using the Gelman-Rubin potential scale reduction factor ( $R$ ) [33]. The calibrated model was obtained by replacing the prior mean parameter values with their corresponding marginal posterior means, together with the remaining uncalibrated parameters set at their default baseline values.

### PK/PD model simulations

Using the calibrated PK/PD model, simulations were run for total lung CFU's (calculated as the product of total bacterial cell density and lung tissue volume) and rifampin concentration in plasma corresponding to the dose-ranging and dose-response studies used for model calibration. A simulation of the experimental dose-fractionation study described in Jayaram et al. [12] was also run to determine a PK/PD model prediction of the PK/PD index which best correlated with bactericidal efficacy. For each dosage regimen in the dose-fractionation simulation, the PK/PD indices;  $AUC_{24}/MIC$ ,  $C_{max}/MIC$ , and  $T_{>MIC}$ , were calculated using the experimentally measured  $MIC = 1\text{mg/L}$  in serum [12], and the model simulated rifampin plasma concentration-time output (making no distinction between plasma and serum measurements). Here,  $MIC$  is the minimum inhibitory concentration,  $AUC_{24}$  is the 24-h area under the concentration-time curve,  $C_{max}$  the peak concentration, and  $T_{>MIC}$  is the percentage of time the plasma concentration exceeds the  $MIC$ . The relationship between the model predicted total lung CFU's and each PK/PD index was summarized by a fit to a sigmoid inhibitory  $E_{max}$  model of the form  $E = E_{max}(1 - X^n/(X_{50}^n + X^n))$ , where  $E$  is the  $\log_{10}$  CFU,  $E_{max}$  is the maximum  $\log_{10}$  CFU reduction,  $X$  is a PK/PD index,  $X_{50}$  is the value of  $X$  at half-maximum effect, and  $n$  is a shape parameter (this is a similar analysis of the model simulated data as was originally applied to the corresponding experimental data). The PK/PD index best characterizing the bactericidal effect was selected as the index with the highest correlation between the fitted  $E_{max}$  equation and the model predicted data, as determined by visual inspection, calculated coefficient of determination,  $R^2$ , and coefficient of variation,  $CV = (\text{root mean square error})/(\text{mean of dependent variable})$ .

To illustrate additional model features of the immune response we simulated the time course of total lung CFU's

together with corresponding cytokine concentrations and macrophage and T cell densities following daily 10 mg/kg oral dosing starting on day 28 post-infection.

### Computational software

MCSim v5.4.0 [34] was used for all PK/PD model simulations, including the MC and MCMC simulations. R v2.15.2 [35], including the CODA package [36], was used for statistical calculations.

## Results

### Calibration

The rifampin PBPK model parameters; fraction of dose absorbed, total clearance, oral absorption rate, and muscle/blood partition coefficient, were shown previously [23] to have the highest correlation with the PBPK model predictions of rifampin plasma concentration, and were included here for calibration to the dose-ranging data. The MC sensitivity analysis for total bacterial cell density was performed with simulations of 6 days/week oral dosing starting on day 28 post-infection. Separate MC simulations were run for each of 1, 30, 90, and 270 mg/kg oral doses. Pearson correlation coefficients between the sampled parameters and predictions of total bacterial cell density were calculated at days 28 and 35 post-infection. Parameters with correlations of absolute value greater than 0.3, at either of the time points and for any of the doses, were considered sensitive. The TB model parameters; bacterial growth rate inside infected macrophages, rate of infection of resting macrophages, saturation for infection of resting macrophages, and maximal carrying capacity of infected macrophages, as well as the drug effect parameter, maximum kill rate for intracellular bacteria, were found to be sensitive for predictions of total bacterial cell density, and were included together with the remaining parameters in the drug-bacteria interaction terms for calibration to the dose-response data.

The baseline mean parameter values that were used to specify the prior distributions for the calibrated PK/PD model parameters are shown in Table 1. The prior mean distributions and summary statistics of the marginal posterior mean distributions are shown for the calibrated PK/PD model parameters in Table 2. For the pharmacokinetic dose-ranging calibration, each of the five Markov chains were generated from 100,000 MCMC iterations, keeping every fifth iteration of the final 10,000. Convergence was obtained as  $R = 1$  for every sampled parameter. The marginal posterior mean values and SD's were calculated from the aggregate of the five chains. While both fraction

**Table 1** PK/PD parameter baseline mean values for Bayesian prior distributions

Parameter (units)	Mean	Source
<b>PBPK model parameters</b>		
$F_a$ Fraction of rifampin dose absorbed	1	[23]
$k_a$ Oral rifampin absorption rate (1/day)	38.64	[23]
$CL_C$ Total rifampin clearance (L/day/kg <sup>0.75</sup> )	0.96	[23]
$P_M$ Rifampin muscle/blood partition coefficient	0.76	[23]
<b>Drug-bacteria parameters</b>		
$f_{LU}$ Fraction of rifampin free in lung	0.3	[12, 23]
$k_{max}^{Ex}$ Maximum kill rate for extracellular bacteria (1/day)	13.82	[12]
$EC_{50}^{Ex}$ Half-maximum effect conc. for extracellular bacteria (mg/L)	1.24	[12]
$\gamma^{Ex}$ Hill coefficient for extracellular bacteria	0.7	[12]
$k_{max}^{In}$ Maximum kill rate for intracellular bacteria (1/day)	1.21	[12]
$EC_{50}^{In}$ Half-maximum effect conc. for intracellular bacteria (mg/L)	3.38	[12]
$\gamma^{In}$ Hill coefficient for intracellular bacteria	0.48	[12]
<b>TB model parameters</b>		
$\alpha_I$ Bacterial growth rate inside infected macrophages (1/day)	0.5	[24]
$k_1$ Rate of infection of resting macrophages (1/day)	0.4	[24]
$c_1$ Saturation for infection of resting macrophages (cell/mL)	10 <sup>6</sup>	[24]
$N$ Maximal carrying capacity of an infected macrophage	25	[24]

**Table 2** Calibration to in vivo dose-ranging and dose–response measurements obtained from Jayaram et al. [12]: prior distributions and posterior distribution summaries

Parameter (units) <sup>a</sup>	Prior	Posterior <sup>b</sup>
<b>PBPK model parameters</b>		
$F_a$	U (0.48, 1.0) <sup>c</sup>	0.59 (0.07)
$k_a$ (1/day)	U (18.0, 59)	36 (10)
$CL_C$ (L/d/kg <sup>0.75</sup> )	U (0.46, 1.5)	0.58 (0.06)
$P_M$	U (0.10, 1.4)	1.1 (0.2)
<b>Drug-bacteria parameters</b>		
$f_{LU}$	U (0.14, 0.46)	0.28 (0.08)
$k_{max}^{Ex}$ (1/day)	U (1.8, 26)	17 (6)
$EC_{50}^{Ex}$ (mg/L)	U (0.17, 2.3)	1.0 (0.6)
$\gamma^{Ex}$	U (0.09, 1.3)	0.62 (0.3)
$k_{max}^{In}$ (1/day)	U (0.16, 2.3)	2.0 (0.2)
$EC_{50}^{In}$ (mg/L)	U (0.45, 6.3)	4.5 (1)
$\gamma^{In}$	U (0.06, 0.9)	0.72 (0.10)
<b>TB model parameters</b>		
$\alpha_I$ (1/day)	U (0.24, 0.76)	0.58 (0.1)
$k_1$ (1/day)	U (0.05, 0.75)	0.55 (0.1)
$c_1$ (cell/mL)	U (1.3 × 10 <sup>5</sup> , 1.9 × 10 <sup>6</sup> )	5.0 × 10 <sup>5</sup> (3 × 10 <sup>5</sup> )
$N$	U (12, 38)	29 (5)

U (a, b); Uniform distribution over [a, b]

<sup>a</sup> Parameter definitions are given in Table 1

<sup>b</sup> Mean(SD)

<sup>c</sup> Truncated to exclude values greater than 1

of dose absorbed and plasma clearance were updated, it is only the ratio  $CL/F$  that is identifiable in the present study, and while each value changed separately from prior to posterior, the prior and posterior ratios remained approximately equal.

The prior baseline mean values of the PBPK model parameters shown in Table 1 were replaced with their corresponding marginal posterior mean values shown in Table 2 for use in the second calibration to the dose–response data. For the calibration to the dose–response data, each of the five Markov chains were generated from 200,000 MCMC iterations, keeping every fifth iteration of the final 10,000. Convergence was obtained as  $R < 1.06$  for every sampled parameter. The marginal posterior mean values and SD’s were calculated from the aggregate of the five chains. The fully calibrated model was obtained using the posterior mean values in Table 2, with the remaining uncalibrated parameters kept at their baseline mean values.

Figure 1 shows simulations of rifampin plasma concentration-time profiles and lung CFU killing kinetics using the calibrated PK/PD model, together with the corresponding mean experimental data from the dose-ranging and dose–response studies in Jayaram et al. [12]. The simulated values of rifampin plasma concentration reasonably approximate the absorption and elimination behavior of the intermediate doses, but show larger deviations from experiment for the low and high doses. The simulation for the 810 mg/kg dose describes the rate of

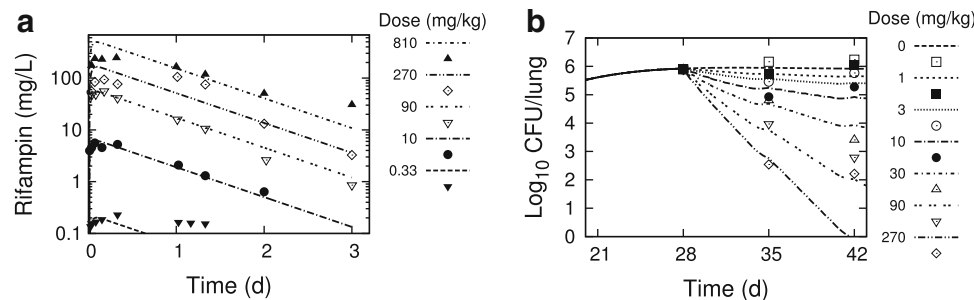


**Fig. 1** Simulations of rifampin in vivo dose-ranging and dose-response studies. The *dashed lines* are simulation outputs, and the data points are replotted experimental data digitally extracted from the corresponding plots in Jayaram et al. [12]. **a** 72-h Rifampin

plasma concentration-time profiles following single oral doses of 0.33, 10, 90, 270, and 810 mg/kg. **b** Total lung CFU's following 6-days/week dosing of 0, 1, 3, 10, 30, 90 and 270 mg/kg, starting day 28 post-infection

elimination, but over-predicts  $C_{max}$ , while the 0.33 mg/kg matches the early absorption data, but over-predicts the rate of elimination. For the dose-response data simulations, the CFU counts on day 28 and the range of CFU counts on day 35 are well simulated by the model, but large deviations from model simulations are evident in the day 42 CFU data points, reflecting the large variation in this experimental data.

### Simulation of dose-fractionation study

The PK/PD model simulation of the dose-fractionation study described in Jayaram et al. [12] consisted of simulations for total lung CFU's on day 34 post-infection, following rifampin dosing starting on day 28 post-infection with total doses of 2, 6, 18, 60, 180, 540, 1080, 1620, 3240, and 4860 mg/kg. Each total dose was fractionated one, three, or six times in 144 h (6 days). For example, the 180 mg/kg total dose was administered as a single dose on day 28, or as 60 mg/kg doses on each of days 28, 30, and 32, or as 30 mg/kg doses on each of days 28 through 33. Single-dose amounts of 1080, 1620, 3240, and 4860 mg/kg, and three-dose amounts of 1080 and 1620 mg/kg, were excluded from the simulations to match the same excluded dosing described in the original experimental study [12].  $AUC_{24}$  was calculated for each dosage regimen by numerical integration of the rifampin plasma concentration-time curve over the 144 h time interval, divided by 6.  $C_{max}$  was identified as the highest predicted rifampin plasma concentration during the 144 h interval.  $T_{>MIC}$  was calculated as the percentage of time the rifampin concentration in plasma was greater than the  $MIC$  over the 144 h interval.

Figure 2 shows the simulation results for model predicted  $\log_{10}$  CFU's plotted against each PK/PD index together with the  $E_{max}$  model fits to the simulation data. Table 3 shows the  $E_{max}$  model and goodness of fit values for the PK/PD model simulated dose-fractionation data and the corresponding experimentally observed data from Jayaram et al. [12]. The

experimental data points used for this analysis were digitally extracted from Fig. 2, Fig. 6B, and Fig. 6C of Jayaram et al. [12]. We note a discrepancy between the same  $AUC/MIC$  data plotted in Fig. 2 and Fig. 6A, with our results in Table 3 conforming to the Fig. 2 in vivo data as the correct values (there was an approximate factor of 5 shift between the data points in each figure with a likely plotting error in the horizontal axis of Fig. 6A). From simulation output for  $AUC_{24}$  and corresponding dose ( $Dose$  (mg/kg)), we determined the relationship  $AUC_{24} = \alpha \cdot Dose$ , where  $\alpha = 11.7, 6.08, \text{ or } 2.08$  (kg/L), for 6, 3, or 1 day/week dosing, respectively. Using this result in the  $E_{max}$  equation for  $AUC_{24}/MIC$  we established the dose-response curves, shown together with the corresponding 6x/week experimental data from Jayaram et al. [12] in Fig. 3.

The pattern of simulated output for the individual mice, and the correlation of PK/PD indices with efficacy in the order  $AUC_{24}/MIC > C_{max}/MIC > T_{>MIC}$ , closely match the experimental results presented in Jayaram et al. [12] (these latter experimental results were not included in our model development or calibration procedure, but were kept as separate independent data used only for comparison to the corresponding computational simulations). While there is overall qualitative agreement between our simulated results and experimental measurement, we find disagreement in the dose fractionation results with a higher than observed prediction of  $AUC_{24}/MIC$  for a 1-log CFU reduction. From our  $E_{max}$  equation for  $AUC_{24}/MIC$ , a 1-log<sub>10</sub> CFU reduction requires  $AUC_{24}/MIC = 368$ ; the corresponding value reported in Jayaram et al. [12] was 271. The difference between these observed and predicted values can be partially attributed to the error in modeling the rifampin plasma concentration-time profiles, most notably seen in the over-prediction of exposure for the higher doses. In the PK/PD correlation analysis of Jayaram et al. [12], the PK plasma exposure values were determined by simulation using a one-compartment model with first-order

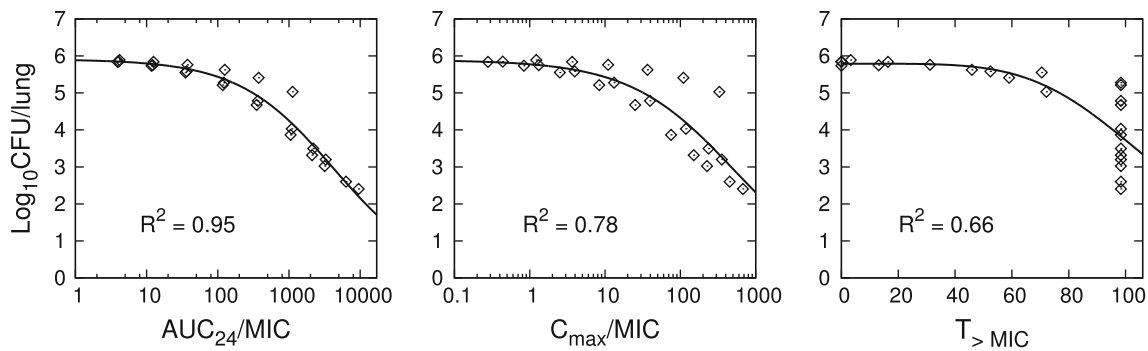


**Fig. 2** PK/PD model simulation of the experimental rifampin dose–fractionation study for TB infected BALB/c mice described in Jayaram et al. [12]. Individual data points (*diamonds*) were PK/PD model generated, with each point obtained from the simulation of

total lung CFU’s and corresponding PK/PD index calculated from simulated plasma concentrations for each dosage regimen of the dose–fractionation study. *Solid lines* are  $E_{max}$  equation fits (Table 2) to the PK/PD model generated data points

**Table 3** Fit of  $E = E_{max}(1 - X^n/(X_{50}^n + X^n))$  to PK/PD model predicted (Fig. 2) and experimentally observed [12] mouse rifampin dose–fractionation data ( $E = \log_{10}$  CFU,  $E_{max}$  = maximum  $E$ ,  $X$  is a PK/PD index,  $X_{50}$  is the value of  $X$  at  $E = E_{max}/2$ , and  $n$  is a shape parameter)

$X$	$E_{max}$		$X_{50}$		$n$		$R^2$		$CV\%$	
	Pred.	Obs.	Pred.	Obs.	Pred.	Obs.	Pred.	Obs.	Pred.	Obs.
$AUC_{24}/MIC$	5.9	5.9	$4.3 \times 10^3$	$3.9 \times 10^3$	0.65	0.70	0.95	0.95	5.4	6.0
$C_{max}/MIC$	5.9	6.2	$5.0 \times 10^2$	$2.8 \times 10^2$	0.63	0.57	0.78	0.81	11	9.1
$T_{> MIC}$	5.8	5.7	$1.1 \times 10^2$	$1.1 \times 10^2$	4.8	11	0.66	0.46	14	18

$R^2$ : coefficient of determination.

$CV\%$ : percent coefficient of variation (of root mean square error).

Pred.: calculated from PK/PD model predicted  $\log_{10}$  CFU versus  $X$  shown in Fig. 2

Obs.: calculated from experimentally observed  $\log_{10}$  CFU versus  $X$  reported in Jayaram et al. [12]

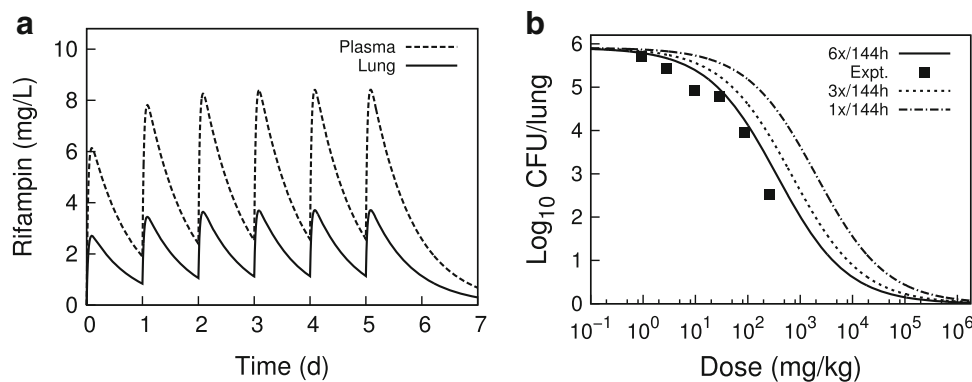


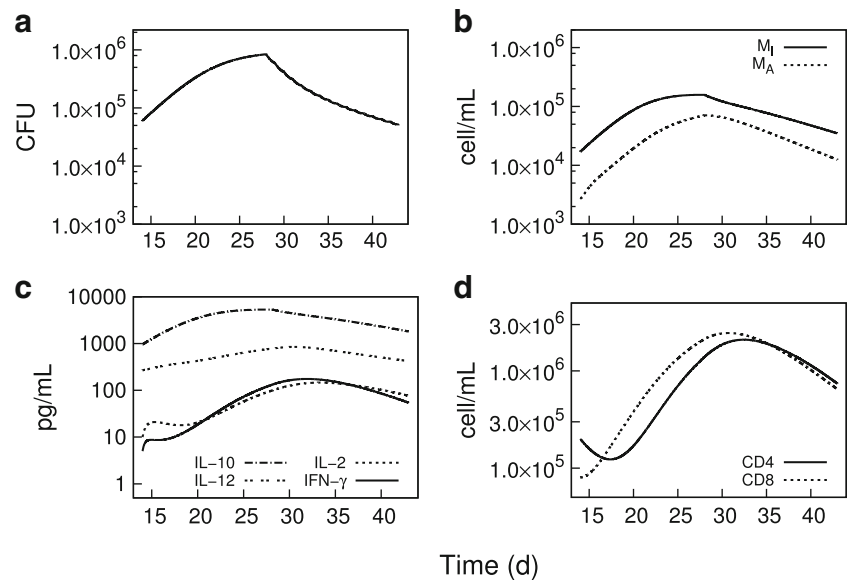
**Fig. 3** PK/PD model simulations. **a** Total rifampin plasma and lung concentration–time profiles following 10 mg/kg, 6x/week daily oral dosing. **b** dose–response curves for reduction in lung CFU counts following 1 week of oral rifampin doses administered 1, 3, or 6 times

in TB-infected BALB/c mice. Experimental data (expt.) digitally extracted and replotted from the corresponding non-zero dosing (6x/week) results in Jayaram et al. [12] (the zero dose value was approximately 6.21  $\log_{10}$ CFU)

absorption and elimination, similar to assumptions made in our PBPK model; as such, we expect similar plasma modeling errors. However, the bacterial killing kinetics were experimental values in Jayaram et al. [12] while here they were model predicted, based on calibration to the

dose–response data in Jayaram et al. [12]. The over-prediction of drug exposure in the high dose measurements would lead to an under-prediction of the true rate of bacterial killing, resulting in over-prediction of exposure necessary for the 1–log CFU reduction.

**Fig. 4** PK/PD model simulations during days 13–44 of pulmonary bacterial load, cytokine concentrations, and macrophage and T cell densities (cells per mL of lung tissue) following a 2-week daily 10 mg/kg oral dose of rifampin beginning on day 28 post-aerosol infection in TB-infected BALB/c mice. **a** Bacterial load (sum of intra- and extra-cellular bacteria). **b** Cell densities of infected ( $M_I$ ) and activated ( $M_A$ ) macrophages. **c** Cytokine (IL-10, IL-2, IL-12, and IFN- $\gamma$ ) concentrations. **d** Cell densities of CD4<sup>+</sup> and CD8<sup>+</sup> T cells



### Simulation of host response

Figure 4 shows the PK/PD model predicted bacterial kinetics and corresponding host response from day 14 through day 42 post-infection, with daily 10 mg/kg rifampin oral dosing beginning on day 28 post-infection. The macrophage cell densities and IL-10 concentration are most clearly seen as directly responsive to the decrease in bacterial load as expected from the location of *M. tuberculosis* primarily in macrophages, and as IL-10 (and IL-12) are secreted by the macrophages. Also, a lag time relative to bacterial load is seen in the response of the T cells and the T cell derived IL-2 and IFN- $\gamma$  cytokines, as expected due to time required for T cells to detect and process regulatory signals from the reduction in bacterial stimuli.

### Discussion

The complexities of anti-TB drug therapy, including host effects and the need for multidrug combinations, strains the capabilities of conventional PK/PD modeling and analysis methods for identifying new optimal regimens. Physiologically based PK/PD modeling can be viewed as a multiscale approach [37] that provides for integration of the multiple aspects of dose-optimization including efficacy, host-toxicity, antimicrobial resistance, and possible drug-drug interactions. PK/PD models for drug treatment of TB that include multiscale descriptions of the host-drug-bacteria interactions are available in the literature [38, 39]. However, while the disease components of these models are physiologically based, the pharmacokinetic components are either empirical models used to describe a single

drug [38], or descriptions of combination therapy using efficacy parameters without consideration of the actual dose or drug concentration kinetics [39]. While these models provide useful insights into drug therapy for TB, we envision a computational framework capable of describing whole-body multidrug PK/PD interactions which requires a more detailed pharmacokinetic description than was used in the available examples. Our objective here was to establish, for a single drug, the essential computational aspects of such a multidrug framework.

We constructed a PK/PD model for rifampin in TB-infected mice by combining models for drug disposition and disease through drug-bacteria interaction terms. The model equations were numerically evaluated in a computational framework that included MC simulations to assess parameter sensitivity, and MCMC simulations for a Bayesian calibration procedure that provided for incorporation of experimental data from in vitro and in vivo measurements. While we considered only a single drug in the present study, the model structure can incorporate multiple drugs through expansion of the pharmacokinetic component to include additional PBPK models for each drug of interest. These separate PBPK models can be linked through tissue and organ compartments that correspond to target sites for PK and PD interactions in a manner described by numerous examples for PBPK modeling of chemical mixtures [28, 40, 41]. As rifampin is a potent cytochrome P450 (CYP) enzyme inducer [42], inclusion of CYP enzyme induction [43] into the present PBPK model and combining with PBPK models for commonly co-administered antiretroviral drugs could serve as an application to modeling dose adjustments required for treatment of TB and human immunodeficiency virus (HIV)



co-infections [44]. The primary aim of accounting for physiological detail in such a modeling framework is to better translate preclinical experimental data to the clinical setting. PBPK modeling is becoming established in drug development through its increasing use for in vitro in vivo extrapolation and interspecies scaling [45]. Additionally, the physiologically based framework described here contains basic modeling elements for novel anti-TB drug therapies such as those related to host-directed adjunct therapies [46] and alternate routes of administration [47].

Our initial application of the computational framework was the simulation of experiments described in a PK/PD study of rifampin in *M. tuberculosis* infected mice [12]. In vitro measurements of protein binding and *M. tuberculosis* killing kinetics in batch culture and in macrophages, together with previously specified PBPK model parameter values, were used to specify prior parameter distributions that were subsequently updated by Bayesian calibration to in vivo dose-ranging and dose–response measurements. While the experimental measurements provided by Jayaram et al. [12] presented an integrated set of data with respect to bacterial strain, mouse models, and methods of analysis; data from separate experiments such as from hollow fiber systems [48] could also be used to inform prior parameter distributions. The parameters chosen for calibration were determined from a ranking of those most sensitive to the experimental data used for calibration and for which experimental measurements were most uncertain. For the PBPK model we restricted calibration to sensitive drug-dependent parameters while leaving the measured drug independent physiological parameters at their baseline values. The calibrated model was used to simulate the experimental dose–fractionation study described in Jayaram et al. [12], with a measured *MIC* incorporated into calculations for the associated PK/PD indices. The simulated output clearly indicated a concentration-dependent behavior, with the  $AUC_{24}/MIC$  best correlating with lung CFU's in agreement with the results in Jayaram et al. [12]. The predicted dose–response curve shown in Fig. 3 (derived from the  $E_{max}$  model fit to  $AUC_{24}/MIC$  simulated data) shows the standard 10 mg/kg dose well below the maximum response, the complete curve showing a wide range over several orders of magnitude for the dose. This result agrees with other experimental studies indicating rifampin under-dosing for TB in mice [49], and illustrates partly the motivation for recent and ongoing high-dose rifampin clinical trials [50, 51].

While the PK/PD model presented here is a first iteration of model development, combining previously disparate mathematical descriptions for the host–drug–bacteria sub-components, these preliminary simulations indicate the utility of a computational PK/PD approach to obtain results that are consistent with an otherwise resource intensive

dose–fractionation experiment. Additionally, consideration of the differences between the PK/PD model predictions and experimental observations provides a means to improve the model and the hypotheses from which the mathematical statements are derived. In conventional PK/PD modeling, differences between prediction and experimental observation are addressed by changes to the model, using alternate variables and parameterizations, without a necessarily corresponding physiological interpretation. For systems-based modeling, changes to the model are constrained by biological and physiological hypotheses and experimentally measured parameter values. In our case, further investigation of the model hypotheses is suggested by the higher than observed prediction of  $AUC_{24}/MIC$  for a 1–log CFU reduction. The PBPK sub-model may be improved, as we discussed in an earlier publication [23], with a more detailed description of enterohepatic circulation that may better simulate the plasma concentration–time profiles. The mathematical TB model [24] was developed to describe early and stationary phase bacterial growth. Experimental data describing drug induced bacterial killing and the simultaneous dynamics of T cells, macrophages, and cytokines is not currently available for mice in the anti-TB drug literature. Such data would be highly beneficial to better test the model predictions and to further understand the host effect during drug treatment.

Two important areas of investigation that were not addressed by our model are the characteristic biphasic killing kinetics observed with prolonged drug treatment [52], and postantibiotic effect (PAE) which refers to delayed regrowth of bacteria after drug exposure [53]. These effects would be important for describing the full time course of anti-TB treatment, including accounting for intermittent or missed doses. PK/PD models for rifampin therapy in human TB described by Goutelle et al. [38], explained the biphasic killing kinetics as arising from an initial rapid killing of a large extracellular bacterial population followed by a slower killing of a protected intracellular sub-population. However, the extracellular bacterial population in standard mouse TB infection models are a much smaller fraction of the total than in humans [54], and preliminary simulations with our PK/PD model (data not shown) do not account adequately for initial rapid killing and longer term persistence. This suggests other mechanisms for bacterial persistence, such as cellular level stochastic processes related to phenotypic heterogeneity [55–57], may be necessary to explain the long-term *M. tuberculosis* killing kinetics in mice. A significant PAE for rifampin against *M. tuberculosis* has been observed in vitro [58], and including a PAE in the model would provide a mechanism for growth inhibition during low or absent drug concentrations. Examples of PK/PD modeling with a PAE are available in the literature [59, 60] and could be included here as a

refinement of our current description of the drug-bacteria interaction.

While systems based modeling may be used to explore a wider range of questions for a particular experimental system than conventional PK/PD modeling, the emphasis on physiological description limits the range of systems to which the model can be applied. The TB infection model [24] was developed using data from standard mouse strains such as C57BL/6 or BALB/c, and would not apply directly to mouse strains with highly differing immune responses, such as gamma-interferon knockout (GKO) mice [61], or the necrotic granuloma forming C3HeB/FeJ [62] mice. The dose, route, and bacterial strain used for infection also play an important role in determining the host immune response [63]. These differences in mouse strain, bacterial strain, and other experimental conditions would require, minimally, modification of initial conditions and various parameter values, together with the appropriate experimental measurements on which to base these modifications. While not implemented in this model, the physiologically based nature of the model parameters provides a mechanism to incorporate mouse intra- and inter-individual variability through MC simulation. Such variability was accounted for previously in the PBPK model [23]; however, information on the variability of the TB model parameters was not provided for the published model used here [24]. Such data would be highly beneficial to better test the model predictions and to further understand the host effect during drug treatment. The motivation to obtain such parameter variability data, as well as data corresponding to immune system components during drug treatment, demonstrates the idea of model-directed experimentation, which provides support for further physiologically based model development and a potential better understanding of the experimental system as a whole.

**Acknowledgments** The authors wish to thank Scott Irwin and Mary Ann De Groote (Colorado State University (CSU)), Joanne Turner (The Ohio State University), and Radha Shandil (formerly AstraZeneca, Bangalore, India) for helpful discussions. The authors also thank Brad Reisfeld and Raymond Yang (CSU) for a careful review and editing of an earlier version of this manuscript. This work was supported by National Institutes of Health Grant Number K25AI089945.

## Appendix

The PK/PD model used in the present work is described by Eqs. (3–23) and the corresponding compartmental structure shown in Fig. 5. The equations are those from Friedman et al. [24] and Lyons et al. [23] together with the modifications described in the “Materials and methods” section.

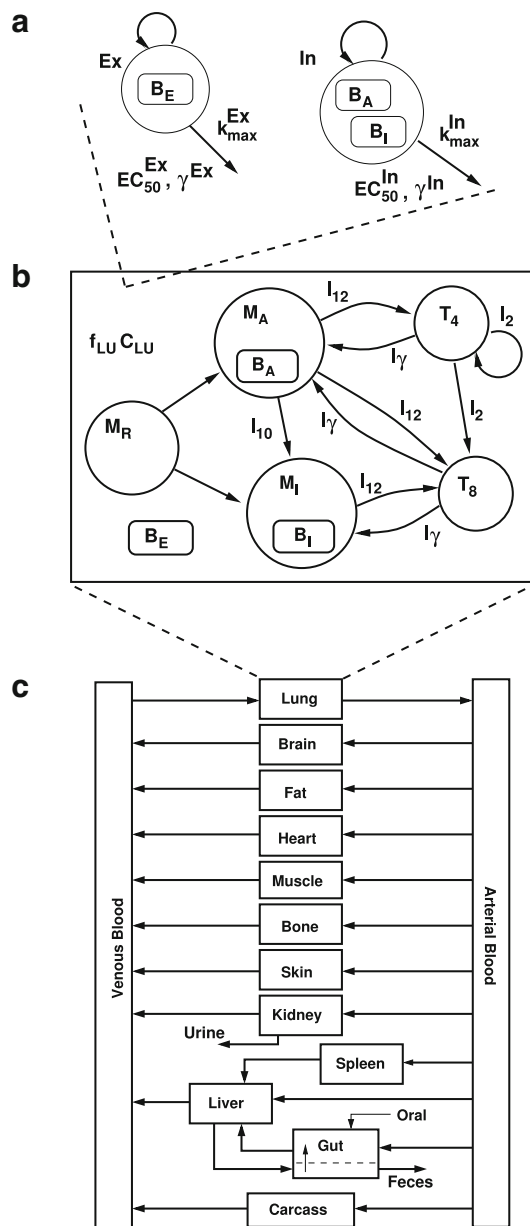


**Fig. 5** PK/PD model structure. **a** Intracellular (In) and extracellular (Ex) bacterial populations and killing kinetics parameters.  $B_E$ : extracellular bacteria,  $B_A$ : bacteria residing in activated macrophages,  $B_I$ : bacteria residing in infected macrophages,  $k_{max}$ : maximum kill rate,  $EC_{50}$ : half-maximum effect drug concentration, and  $\gamma$ : Hill coefficient. **b** Lung compartment with free rifampin drug concentration ( $f_{LU}C_{LU}$ ) together with cell and cytokine populations (adapted from Friedman et al. [24]).  $M_R$ ,  $M_A$ , and  $M_I$ : resting, activated, and infected macrophages.  $I_{10}$ ,  $I_{12}$ ,  $I_2$ , and  $I_\gamma$ : IL-10, IL-12, IL-2, and IFN- $\gamma$ .  $T_4$  and  $T_8$ : CD4 $^+$  and CD8 $^+$  T cells. **c** Rifampin PBPK model compartments and blood flow (adapted from Lyons et al. [23])

## Pharmacodynamics: TB model

The TB model and drug-bacteria interactions are described by Eqs. (3–13). The variable names, descriptions, and initial

conditions used in the the present work are shown in Table 4. The parameter values that were not updated in the Bayesian calibration are shown in Table 5, while the updated parameters are the posterior mean values shown in Table 2.

$$\begin{aligned} \frac{dB_I}{dt} = & \alpha_I B_I \left( 1 - \frac{B_I^2}{B_I^2 + (NM_I)^2} \right) + k_1 n_3 M_R \frac{B_E}{B_E + c_1} \\ & - k_2 NM_I \frac{B_I^2}{B_I^2 + (NM_I)^2} \\ & - n_1 k_3 B_I \frac{I_\gamma}{I_\gamma + c_2} + n_2 k_4 B_A \frac{I_{10}}{I_{10} + c_3 I_\gamma + c_4} \\ & - B_I \frac{k_{max}^{In} (f_{LU} C_{LU})^{\gamma^{In}}}{(EC_{50}^{In})^{\gamma^{In}} + (f_{LU} C_{LU})^{\gamma^{In}}} \end{aligned} \tag{3}$$

$$\begin{aligned} \frac{dB_A}{dt} = & \alpha_A B_A - n_2 k_4 B_A \frac{I_{10}}{I_{10} + c_3 I_\gamma + c_4} + n_1 k_3 B_I \frac{I_\gamma}{I_\gamma + c_2} \\ & - n_2 \mu_{MA} B_A - B_A \frac{k_{max}^{In} (f_{LU} C_{LU})^{\gamma^{In}}}{(EC_{50}^{In})^{\gamma^{In}} + (f_{LU} C_{LU})^{\gamma^{In}}} \end{aligned} \tag{4}$$

$$\begin{aligned} \frac{dB_E}{dt} = & \alpha_E B_E - k_1 n_3 M_R \frac{B_E}{B_E + c_1} + k_2 NM_I \frac{B_I^2}{B_I^2 + (NM_I)^2} \\ & - k_5 M_A B_E + n_2 \mu_{MA} B_A - B_E \frac{k_{max}^{Ex} (f_{LU} C_{LU})^{\gamma^{Ex}}}{(EC_{50}^{Ex})^{\gamma^{Ex}} + (f_{LU} C_{LU})^{\gamma^{Ex}}} \end{aligned} \tag{5}$$

$$\begin{aligned} \frac{dM_I}{dt} = & k_1 M_R \frac{B_E}{B_E + c_1} - k_2 M_I \frac{B_I^2}{B_I^2 + (NM_I)^2} - k_3 M_I \frac{I_\gamma}{I_\gamma + c_2} \\ & + k_4 M_A \frac{I_{10}}{I_{10} + c_3 I_\gamma + c_4} - \mu_{MI} M_I \end{aligned} \tag{6}$$

$$\begin{aligned} \frac{dM_A}{dt} = & - k_4 M_A \frac{I_{10}}{I_{10} + c_3 I_\gamma + c_4} + k_3 M_I \frac{I_\gamma}{I_\gamma + c_2} - \mu_{MA} M_A \\ & + k_6 M_R \frac{B_E}{B_E + c_5} \frac{I_\gamma}{I_\gamma + c_6} \end{aligned} \tag{7}$$

$$\frac{dI_{10}}{dt} = k_7 M_I \frac{c_7}{I_{10} + c_7} - \mu_{10} I_{10} \tag{8}$$

$$\frac{dI_{12}}{dt} = k_8 M_A \frac{c_8}{I_{10} + c_8} + k_9 M_R \frac{B_E}{B_E + c_9} - \mu_{12} I_{12} \tag{9}$$

$$\frac{dI_2}{dt} = k_{10} T_4 - (k_{11} T_4 + k_{12} T_8) \frac{I_2}{I_2 + c_{10}} - \mu_2 I_2 \tag{10}$$

$$\frac{dI_\gamma}{dt} = (\lambda_u(t) T_4 + \lambda_y(t) T_8) \frac{I_{12}}{I_{12} + c_{11}} - \mu_\gamma I_\gamma \tag{11}$$

$$\frac{dT_4}{dt} = \lambda_z(t) M_A I_{12} + k_{13} T_4 \frac{I_2}{I_2 + c_{10}} - \mu_{T4} T_4 \tag{12}$$

$$\frac{dT_8}{dt} = \lambda_x(t) (M_A + M_I) I_{12} + k_{14} T_8 \frac{I_2}{I_2 + c_{10}} - \mu_{T8} T_8 \tag{13}$$

The functions  $\lambda_i(t)$ ,  $i = \{x, y, z, u\}$  were implemented here as  $\lambda_i(t) = \lambda_i \cdot \theta(t - t_{delay})$ , where  $t_{delay} = 14$  days, and  $\theta(x) = 1(0)$  for  $x \geq 0(x < 0)$  is a step function.

**Pharmacokinetics: PBPK model**

The PBPK model is described by Eqs. (14–23) with initial conditions all set to zero. The subscripts,  $T$ , on the tissue volumes,  $V_T$ , drug concentrations,  $C_T$ , blood flow rates,  $Q_T$ , and tissue/blood partition coefficients,  $P_T$ , denote abbreviations for the model compartments as;  $V$ : venous blood,  $LU$ : lung,  $A$ : arterial blood,  $BR$ : brain,  $F$ : fat,  $SK$ : skin,  $K$ : kidney,  $S$ : spleen,  $G$ : gut,  $GL$ : gut lumen,  $L$ : liver,  $LA$ : hepatic artery,  $CR$ : carcass. Fractional tissue volumes,  $V_{TC}$ , and blood flow rates,  $Q_{TC}$ , were scaled to total values as  $V_T = V_{TC} \cdot BW$  and  $Q_T = Q_{CC} \cdot BW^{0.75}$ .  $BW$  is body weight, and  $Q_{CC}$  is an allometric coefficient for cardiac output. Fractional clearance was also scaled as  $CL = CL_C \cdot BW^{0.75}$ . Drug concentration in plasma was determined from concentration in venous blood as  $C_{plasma} = C_V / BP$ . The parameter values that were not updated in the Bayesian calibration are shown in Tables 6 and 7, while the updated parameters are given in Table 2.

**Table 4** PD model variables and initial conditions (day 7 post-infection) used in the present work. The variable names, descriptions, and values are from Friedman et al. [24]

Variable (units)		Value
$B_I$	Density of bacteria residing in infected macrophages (cell/mL)	36,000
$B_A$	Density of bacteria residing in activated macrophages (cell/mL)	1000
$B_E$	Density of extracellular bacteria (cell/mL)	1000
$M_I$	Density of infected macrophages (cell/mL)	1800
$M_A$	Density of activated macrophages (cell/mL)	200
$M_R$	Density of resting macrophages (cell/mL)	$5 \times 10^5$
$I_{10}$	Concentration of IL-10 (pg/mL)	100
$I_{12}$	Concentration of IL-12 (pg/mL)	50
$I_2$	Concentration of IL-2 (pg/mL)	10
$I_\gamma$	Concentration of IFN- $\gamma$ (pg/mL)	5
$T_4$	Density of CD4 <sup>+</sup> T cells (cell/mL)	$2 \times 10^5$
$T_8$	Density of CD8 <sup>+</sup> T cells (cell/mL)	$8 \times 10^4$

**Table 5** Baseline PD model parameters that were not updated in the Bayesian calibration procedure. The parameter names, descriptions, and values are from Friedman et al. [24]

Parameter (units)	Value	
$\alpha_E$	Growth rate of $B_E$ (1/day)	0
$\alpha_A$	Growth rate of $B_A$ (1/day)	0
$k_2$	Burst rate of infected macrophages (1/day)	0.81139
$k_3$	Activation rate of infected macrophages (1/day)	0.023415
$k_4$	Deactivation rate of activated macrophages (1/day)	0.28876
$k_5$	Take up of $B_E$ by activated macrophages (mL/cell/day)	$8.1301 \times 10^{-5}$
$k_6$	Rate of activation of resting macrophages (1/day)	0.077068
$k_7$	IL-10 production rate by infected macrophages (pg/mL/cell)	0.50610
$k_8$	IL-12 production rate by activated macrophages (pg/cell/day)	0.28503
$k_9$	IL-12 production rate by resting macrophages (pg/cell/day)	$5 \times 10^{-4}$
$k_{10}$	IL-2 production rate by $T_4$ (pg/cell/day)	$2.1873 \times 10^{-4}$
$k_{11}$	Loss of IL-2 due to proliferation of $T_4$ (pg/cell/day)	$1.6383 \times 10^{-4}$
$k_{12}$	Loss of IL-2 due to proliferation of $T_8$ (pg/cell/day)	$1.6383 \times 10^{-5}$
$k_{13}$	Rate of proliferation of $T_4$ by IL-2 (mL/pg/day)	0.16383
$k_{14}$	Rate of proliferation of $T_8$ by IL-2 (mL/pg/day)	0.016383
$c_2$	Saturation for activation of infected macrophages (pg/mL)	50
$c_3$	IFN- $\gamma$ inhibition for deactivation of activated macrophages	3
$c_4$	Saturation for deactivation of activated macrophages (pg/mL)	1
$c_5$	Saturation for activation of resting macrophages (cell/mL)	$10^5$
$c_6$	IFN- $\gamma$ saturation for activation of resting macrophages (pg/mL)	20
$c_7$	Saturation for IL-10 inhibition by IL-10 (pg/mL)	5000
$c_8$	Saturation for IL-12 inhibition by IL-10 (pg/mL)	200
$c_9$	Saturation for IL-12 production by resting macrophages (cell/mL)	5000
$c_{10}$	Saturation for T cell proliferation by IL-2 (pg/mL)	50
$c_{11}$	Saturation for IFN- $\gamma$ production by T cells and IL-12 (cell/mL)	50
$n_1$	Average number of $B_I$ in an infected macrophage	20
$n_2$	Average number of $B_A$ in an activated macrophage	5
$n_3$	Threshold at which a resting macrophage becomes infected	10
$\mu_{MA}$	Death rate of activated macrophages (1/day)	0.015
$\mu_{MI}$	Death rate of infected macrophages (1/day)	0.2
$\mu_{10}$	Decay rate of IL-10 (1/day)	7.23
$\mu_{12}$	Decay rate of IL-12 (1/day)	1.188
$\mu_2$	Decay rate of IL-2 (1/day)	1.188
$\mu_\gamma$	Decay rate of IFN- $\gamma$ (1/day)	3
$\mu_{T4}$	Death rate of $T_4$ (1/day)	0.33
$\mu_{T8}$	Death rate of $T_8$ (1/day)	0.33
$\lambda_u$	Rate of IFN- $\gamma$ production by $T_4$ (pg/cell/day)	$1.24 \times 10^{-4}$
$\lambda_y$	Rate of IFN- $\gamma$ production by $T_8$ (pg/cell/day)	$1.24 \times 10^{-4}$
$\lambda_z$	Rate of MHCII activation (mL/pg/day)	0.010532
$\lambda_x$	Rate of MHCI activation (mL/pg/day)	0.005266

$$V_V \frac{dC_V}{dt} = \sum_T Q_T C_T / P_T - Q_C C_V, \tag{14}$$

$$T = \{BR, F, H, M, B, SK, K, L, CR\}$$

$$V_T \frac{dC_T}{dt} = Q_T (C_V - C_T / P_T), \tag{17}$$

$$T = \{BR, F, H, M, B, SK, S, CR\}$$

$$V_{LU} \frac{dC_{LU}}{dt} = Q_C (C_V - C_{LU} / P_{LU}) \tag{15}$$

$$V_K \frac{dC_K}{dt} = Q_K (C_A - C_K / P_K) - f_R \cdot CL \cdot C_A \tag{18}$$

$$V_A \frac{dC_A}{dt} = Q_C (C_{LU} / P_{LU} - C_A) \tag{16}$$

$$V_L \frac{dC_L}{dt} = Q_{LA} C_A + Q_S C_S / P_S + C_G Q_G / P_G - Q_L C_L / P_L \tag{19}$$

**Table 6** Baseline anatomical/physiological PBPK model parameters that were not updated in the Bayesian calibration procedure

Parameter (units)	Value
$Q_{CC}$	Cardiac output (L/day/kg <sup>0.75</sup> ) 396
$k_F$	Gut lumen transit rate (1/day) 14.4
Fractional tissue volumes <sup>a</sup>	
$V_{LUC}$	Lung 0.007
$V_{BRC}$	Brain 0.017
$V_{FC}$	Fat 0.07
$V_{HC}$	Heart 0.005
$V_{MC}$	Muscle 0.384
$V_{BC}$	Bone 0.107
$V_{SKC}$	Skin 0.165
$V_{KC}$	Kidney 0.017
$V_{SC}$	Spleen 0.0035
$V_{GC}$	Gut 0.042
$V_{LC}$	Liver 0.055
$V_{VC}$	Venous blood 0.0327
$V_{AC}$	Arterial blood 0.0163
$V_{CRC}$	Carcass 0.0785
Fractional blood flows <sup>b</sup>	
$Q_{BRC}$	Brain 0.033
$Q_{FC}$	Fat 0.09
$Q_{HC}$	Heart 0.066
$Q_{MC}$	Muscle 0.159
$Q_{BC}$	Bone 0.11
$Q_{SKC}$	Skin 0.058
$Q_{KC}$	Kidney 0.091
$Q_{SC}$	Spleen 0.01
$Q_{GC}$	Gut 0.13
$Q_{LAC}$	Hepatic artery 0.02
$Q_{CRC}$	Carcass 0.233

The parameter names, descriptions, and values are from Lyons et al. [23]

<sup>a</sup> Fraction of body weight

<sup>b</sup> Fraction of cardiac output

$$-(1 - f_R) \cdot CL \cdot (Q_{LA}C_A + Q_S C_S / P_S + Q_G C_G / P_G) / Q_L \tag{20}$$

$$V_G \frac{dC_G}{dt} = Q_G(C_A - C_G / P_G) + k_a A_{OD} + k_r A_{GL} \tag{21}$$

$$\frac{dA_{GL}}{dt} = (1 - f_R) \cdot CL \cdot (Q_{LA}C_A + Q_S C_S / P_S + Q_G C_G / P_G) / Q_L - (k_r + k_F) A_{GL} \tag{22}$$

$$\frac{dA_{OD}}{dt} = -k_a \cdot A_{OD} + F_a \cdot D \cdot \sum_{n=0} \delta(t - t_n) \tag{23}$$

The summation in Eq. (14) is over all tissues draining into the venous blood compartment; for liver,

**Table 7** Baseline rifampin-dependent PBPK model parameters that were not updated in the Bayesian calibration procedure

Parameter (units)	Value
$f_R$	Fractional renal clearance 0.19
$k_r$	Gut reabsorption rate (1/day) 4.08
Partition coefficients	
$BP$	Blood/plasma 0.9
$P_{LU}$	Lung/blood 0.49
$P_{BR}$	Brain/blood 0.11
$P_F$	Fat/blood 0.34
$P_H$	Heart/blood 0.74
$P_B$	Bone/blood 0.22
$P_{SK}$	Skin/blood 0.76
$P_K$	Kidney/blood 0.59
$P_S$	Spleen/blood 0.25
$P_G$	Gut/blood 0.74
$P_L$	Liver/blood 3.1
$P_{CR}$	Carcass/blood 0.59

The parameter names, descriptions, and values are from Lyons et al. [23]

$Q_L = (Q_{LA} + Q_S + Q_G)$ . The symbols  $A_{OD}$  and  $A_{GL}$  in Eqs. (21–23) are the amounts of drug input to the gut and in the gut lumen. The delta function in Eq. (23) describes pulsed oral bolus dosing ( $D = \text{dose}$ ), with times of administration,  $t_n, n = 0, \dots, n_{max} - 1$ , with  $n_{max}$  the maximum number of doses in the treatment interval.

## References

1. Laurenzi M, Ginsberg A, Spigelman M (2007) Challenges associated with current and future TB treatment. *Infect Disord Drug Targets* 7(2):105–119
2. Spigelman M, Woosley R, Gheuens J (2010) New initiative speeds tuberculosis drug development: novel drug regimens become possible in years, not decades. *Int J Tuberc Lung Dis* 14(6):663–664
3. Nuermberger E, Tyagi S, Tasneen R, Williams KN, Almeida D, Rosenthal I, Grosset JH (2008) Powerful bactericidal and sterilizing activity of a regimen containing PA-824, moxifloxacin, and pyrazinamide in a murine model of tuberculosis. *Antimicrob Agents Chemother* 52(4):1522–1524
4. Tasneen R, Li SY, Peloquin CA, Taylor D, Williams KN, Andries K, Mdluli KE, Nuermberger EL (2011) Sterilizing activity of novel TMC207- and PA-824-containing regimens in a murine model of tuberculosis. *Antimicrob Agents Chemother* 55(12):5485–5492
5. Williams K, Minkowski A, Amoabeng O, Peloquin CA, Taylor D, Andries K, Wallis RS, Mdluli KE, Nuermberger EL (2012) Sterilizing activities of novel combinations lacking first- and second-line drugs in a murine model of tuberculosis. *Antimicrob Agents Chemother* 56(6):3114–3120
6. Diacon AH, Dawson R, von Groote-Bidlingmaier F, Symons G, Venter A, Donald PR, van Niekerk C, Everitt D, Winter H, Becker P, Mendel CM, Spigelman MK (2012) 14-day

- bactericidal activity of PA-824, bedaquiline, pyrazinamide, and moxifloxacin combinations: a randomised trial. *Lancet* 380(9846):986–993
7. Mouton JW, Ambrose PG, Canton R, Drusano GL, Harbarth S, MacGowan A, Theuretzbacher U, Turnidge J (2011) Conserving antibiotics for the future: new ways to use old and new drugs from a pharmacokinetic and pharmacodynamic perspective. *Drug Resist Updat* 14(2):107–117
  8. Chang KC, Leung CC, Grosset J, Yew WW (2011) Treatment of tuberculosis and optimal dosing schedules. *Thorax* 66(11):997–1007
  9. De Groot MA, Gruppo V, Woolhiser LK, Orme IM, Gilliland JC, Lenaerts AJ (2012) Importance of confirming data on the in vivo efficacy of novel antibacterial drug regimens against various strains of *Mycobacterium tuberculosis*. *Antimicrob Agents Chemother* 56(2):731–738
  10. Grosset J, Almeida D, Converse PJ, Tyagi S, Li SY, Ammerman NC, Pym AS, Wallengren K, Hafner R, Lalloo U, Swindells S, Bishai WR (2012) Modeling early bactericidal activity in murine tuberculosis provides insights into the activity of isoniazid and pyrazinamide. *Proc Natl Acad Sci USA* 109(37):15,001–15,005
  11. Ginsberg A (2011) The TB Alliance: overcoming challenges to chart the future course of TB drug development. *Future Med Chem* 3(10):1247–1252
  12. Jayaram R, Gaonkar S, Kaur P, Suresh BL, Mahesh BN, Jayashree R, Nandi V, Bharat S, Shandil RK, Kantharaj E, Balasubramanian V (2003) Pharmacokinetics-pharmacodynamics of rifampin in an aerosol infection model of tuberculosis. *Antimicrob Agents Chemother* 47(7):2118–2124
  13. Jayaram R, Shandil RK, Gaonkar S, Kaur P, Suresh BL, Mahesh BN, Jayashree R, Nandi V, Bharath S, Kantharaj E, Balasubramanian V (2004) Isoniazid pharmacokinetics-pharmacodynamics in an aerosol infection model of tuberculosis. *Antimicrob Agents Chemother* 48(8):2951–2957
  14. Shandil RK, Jayaram R, Kaur P, Gaonkar S, Suresh BL, Mahesh BN, Jayashree R, Nandi V, Bharath S, Balasubramanian V (2007) Moxifloxacin, ofloxacin, sparfloxacin, and ciprofloxacin against *Mycobacterium tuberculosis*: evaluation of in vitro and pharmacodynamic indices that best predict in vivo efficacy. *Antimicrob Agents Chemother* 51(2):576–582
  15. Pasipanodya J, Gumbo T (2011) An oracle: antituberculosis pharmacokinetics-pharmacodynamics, clinical correlation, and clinical trial simulations to predict the future. *Antimicrob Agents Chemother* 55(1):24–34
  16. Ahmad Z, Peloquin CA, Singh RP, Derendorf H, Tyagi S, Ginsberg A, Grosset JH, Nuermberger EL (2011) PA-824 exhibits time-dependent activity in a murine model of tuberculosis. *Antimicrob Agents Chemother* 55(1):239–245
  17. Tasneen R, Williams K, Amoabeng O, Minkowski A, Mdluli KE, Upton AM, Nuermberger EL (2015) Contribution of the nitroimidazoles PA-824 and TBA-354 to the activity of novel regimens in murine models of tuberculosis. *Antimicrob Agents Chemother* 59(1):129–135
  18. Meibohm B, Derendorf H (1997) Basic concepts of pharmacokinetic/pharmacodynamic (PK/PD) modelling. *Int J Clin Pharmacol Ther* 35(10):401–413
  19. Katsube T, Yamano Y, Yano Y (2008) Pharmacokinetic-pharmacodynamic modeling and simulation for in vivo bactericidal effect in murine infection model. *J Pharm Sci* 97(4):1606–1614
  20. Katsube T, Yano Y, Yamano Y, Munekage T, Kuroda N, Takano M (2008) Pharmacokinetic-pharmacodynamic modeling and simulation for bactericidal effect in an in vitro dynamic model. *J Pharm Sci* 97(9):4108–4117
  21. Nielsen EI, Cars O, Friberg LE (2011) Pharmacokinetic/pharmacodynamic (PK/PD) indices of antibiotics predicted by a semimechanistic PKPD model: a step toward model-based dose optimization. *Antimicrob Agents Chemother* 55(10):4619–4630
  22. Tan YM, Clewell H, Campbell J, Andersen M (2011) Evaluating pharmacokinetic and pharmacodynamic interactions with computational models in supporting cumulative risk assessment. *Int J Environ Res Public Health* 8(5):1613–1630
  23. Lyons MA, Reisfeld B, Yang RS, Lenaerts AJ (2013) A physiologically based pharmacokinetic model of rifampin in mice. *Antimicrob Agents Chemother* 57(4):1763–1771
  24. Friedman A, Turner J, Szomolay B (2008) A model on the influence of age on immunity to infection with *Mycobacterium tuberculosis*. *Exp Gerontol* 43(4):275–285
  25. Vaddady PK, Lee RE, Meibohm B (2010) In vitro pharmacokinetic/pharmacodynamic models in anti-infective drug development: focus on TB. *Future Med Chem* 2(8):1355–1369
  26. Charles River Laboratories Inc (2006) Charles River Laboratories Research Models & Services. <http://www.criver.com>
  27. Gibaldi M, Perrier D (1982) *Pharmacokinetics*. Marcel Dekker Inc, New York
  28. Cheng S, Bois FY (2011) A mechanistic modeling framework for predicting metabolic interactions in complex mixtures. *Environ Health Perspect* 119(12):1712–1718
  29. Bernillon P, Bois FY (2000) Statistical issues in toxicokinetic modeling: a Bayesian perspective. *Environ Health Perspect* 108(Suppl 5):883–893
  30. Frantz J (2012) G3data, version 1.5.2, Software. <https://github.com/pn2200/g3data.git>
  31. Bauer B, Reynolds M (2008) Recovering data from scanned graphs: performance of Frantz's g3data software. *Behav Res Methods* 40(3):858–868
  32. Chiu WA, Okino MS, Evans MV (2009) Characterizing uncertainty and population variability in the toxicokinetics of trichloroethylene and metabolites in mice, rats, and humans using an updated database, physiologically based pharmacokinetic (PBPK) model, and Bayesian approach. *Toxicol Appl Pharmacol* 241(1):36–60
  33. Gelman A, Carlin JB, Stern HS, Rubin DB (2003) *Bayesian data analysis*, 2nd edn. Chapman and Hall/CRC, Boca Raton
  34. Bois FY, Maszle DR (1997) MCSim: a Monte Carlo simulation program. *J Stat Softw* 2(i09):1–60
  35. R Core Team (2012) R: a language and environment for statistical computing. R Foundation for Statistical Computing, Vienna, Austria. <http://www.R-project.org>
  36. Plummer M, Best N, Cowles K, Vines K (2006) CODA: convergence diagnosis and output analysis for MCMC. *R News* 6(1):7–11
  37. van der Graff PH, Benson N (2011) Systems pharmacology: bridging systems biology and pharmacokinetics-pharmacodynamics (PKPD) in drug discovery and development. *Pharm Res* 28(7):1460–1464
  38. Goutelle S, Bourguignon L, Jelliffe RW, Conte JE, Maire P (2011) Mathematical modeling of pulmonary tuberculosis therapy: Insights from a prototype model with rifampin. *J Theor Biol* 282(1):80–92
  39. Magombedze G, Garira W, Mwenje E (2006) Mathematical modeling of chemotherapy of human TB infection. *J Biol Syst* 14:509–553
  40. Yang RS, El-Masri HA, Thomas RS, Dobrev ID, Dennison JE, Bae DS, Campain JA, Liao KH, Reisfeld B, Andersen ME, Mumtaz M (2004) Chemical mixture toxicology: from descriptive to mechanistic, and going on to in silico toxicology. *Environ Toxicol Pharmacol* 18(2):65–81
  41. Mumtaz M, Fisher J, Blount B, Ruiz P (2012) Application of physiologically based pharmacokinetic models in chemical risk assessment. *J Toxicol* 904:603

42. Baciewicz AM, Chrisman CR, Finch CK, Self TH (2013) Update on rifampin, rifabutin, and rifapentine drug interactions. *Curr Med Res Opin* 29(1):1–12
43. Raybon JJ, Pray D, Morgan DG, Zoeckler M, Zheng M, Sinz M, Kim S (2011) Pharmacokinetic-pharmacodynamic modeling of rifampicin-mediated Cyp3a11 induction in steroid and xenobiotic X receptor humanized mice. *J Pharmacol Exp Ther* 337(1):75–82
44. Dooley KE, Flexner C, Andrade AS (2008) Drug interactions involving combination antiretroviral therapy and other anti-infective agents: repercussions for resource-limited countries. *J Infect Dis* 198(7):948–961
45. Rowland M, Peck C, Tucker G (2011) Physiologically-based pharmacokinetics in drug development and regulatory science. *Annu Rev Pharmacol Toxicol* 51:45–73
46. Gonzalez-Juarrero M (2012) Immunity to TB and targets for immunotherapy. *Immunotherapy* 4(2):187–199
47. Gonzalez-Juarrero M, Woolhiser LK, Brooks E, DeGroot MA, Lenaerts AJ (2012) Mouse model for efficacy testing of anti-tuberculosis agents via intrapulmonary delivery. *Antimicrob Agents Chemother* 56(7):3957–3959
48. Srivastava S, Gumbo T (2011) In vitro and in vivo modeling of tuberculosis drugs and its impact on optimization of doses and regimens. *Curr Pharm Des* 17(27):2881–2888
49. de Steenwinkel JE, Aarnoutse RE, de Kneegt GJ, Ten Kate MT, Teulen M, Verbrugh HA, Boeree MJ, van Soolingen D, Bakker-Woudenberg IA (2013) Optimization of the rifampin dosage to improve the therapeutic efficacy in tuberculosis treatment, using a murine model. *Am J Respir Crit Care Med* 187(10):1127–1134
50. Radboud University (2013) Pharmacokinetics and pharmacodynamics of high versus standard dose rifampicin in patients with pulmonary tuberculosis (High RIF). In: <http://www.ClinicalTrials.gov> [Internet], Bethesda (MD): National Library of Medicine (US). Available from: <http://www.clinicaltrials.gov/ct2/show/results/NCT00760149>, nLM Identifier: NCT00760149
51. Radboud University (2014) Safety, tolerability, extended early bactericidal activity and PK of higher doses rifampicin in adults with pulmonary TB (HR1) In: <http://www.ClinicalTrials.gov> [Internet], Bethesda (MD): National Library of Medicine (US). Available from: <http://clinicaltrials.gov/ct2/show/results/NCT00760149>, nLM Identifier: NCT00760149
52. McCune RM, Tompsett R (1956) Fate of *Mycobacterium tuberculosis* in mouse tissues as determined by the microbial enumeration technique. I. The persistence of drug-susceptible tubercle bacilli in the tissues despite prolonged antimicrobial therapy. *J Exp Med* 104(5):737–762
53. Craig WA (1998) Pharmacokinetic/pharmacodynamic parameters: rationale for antibacterial dosing of mice and men. *Clin Infect Dis* 26(1):1–10
54. Hoff DR, Ryan GJ, Driver ER, Ssemakulu CC, De Groot MA, Basaraba RJ, Lenaerts AJ (2011) Location of intra- and extracellular *M. tuberculosis* populations in lungs of mice and guinea pigs during disease progression and after drug treatment. *PLoS One* 6(3):e17550
55. Dhar N, McKinney JD (2007) Microbial phenotypic heterogeneity and antibiotic tolerance. *Curr Opin Microbiol* 10(1):30–38
56. Rocco A, Kierzek AM, McFadden J (2013) Slow protein fluctuations explain the emergence of growth phenotypes and persistence in clonal bacterial populations. *PLoS One* 8(1):e54272
57. Wakamoto Y, Dhar N, Chait R, Schneider K, Signorino-Gelo F, Leibler S, McKinney JD (2013) Dynamic persistence of antibiotic-stressed mycobacteria. *Science* 339(6115):91–95
58. Gumbo T, Louie A, Deziel MR, Liu W, Parsons LM, Salfinger M, Drusano GL (2007) Concentration-dependent *Mycobacterium tuberculosis* killing and prevention of resistance by rifampin. *Antimicrob Agents Chemother* 51(11):3781–3788
59. Geli P, Andersson M, Svensson A, Andersson DI (2009) A multi-type branching model with varying environment for bacterial dynamics with postantibiotic effect. *J Theor Biol* 256(1):58–64
60. Geli P (2009) Modeling the mechanism of postantibiotic effect and determining implications for dosing regimens. *J Math Biol* 59(5):717–728
61. Lenaerts AJ, Gruppo V, Brooks JV, Orme IM (2003) Rapid in vivo screening of experimental drugs for tuberculosis using gamma interferon gene-disrupted mice. *Antimicrob Agents Chemother* 47(2):783–785
62. Pan H, Yan BS, Rojas M, Shebzukhov YV, Zhou H, Kobzik L, Higgins DE, Daly MJ, Bloom BR, Kramnik I (2005) Ipr1 gene mediates innate immunity to tuberculosis. *Nature* 434(7034):767–772
63. Flynn JL (2006) Lessons from experimental *Mycobacterium tuberculosis* infections. *Microbes Infect* 8(4):1179–1188